Dielectric permittivity of C-S-H

Sofiane Ait Hamadouche, Tulio Honorio, Thierry Bore, Farid Benboudjema, Franck Daout, Eric Vourc'H

Dielectric permittivity of C-S-H

Sofiane Ait Hamadouche[a,b,*], Tulio Honorio[a], Thierry Bore[c], Farid Benboudjema[a], Franck Daout[b], Eric Vourc'h[b]

[a] *Université Paris-Saclay, CentraleSupélec, ENS Paris-Saclay, CNRS, LMPS - Laboratoire de Mécanique Paris-Saclay, 91190, Gif-sur-Yvette, France.*
[b] *SATIE, UMR CNRS 8029, ENS Paris Saclay, Université Paris Saclay, Gif-sur-Yvette, France.*
[c] *School of Civil Engineering, The University of Queensland, St Lucia, QLD 4072, Australia.*

Abstract

As a porous hydrophilic phase, C-S-H is expected to exhibit a frequency-dependent dielectric response. This C-S-H property remains unknown, despite the importance of dielectric assessment for non-destructive evaluation of concrete. This study adopts a multiscale approach to estimate the complex dielectric response of C-S-H over the [0; 1000 GHz] frequency range. We perform molecular dynamics simulations to compute the frequency-dependent dielectric response of water in C-S-H from the polarization correlation formula. We consider pore sizes covering the range associated with interlayer and gel pores in C-S-H. The dielectric response obtained is anisotropic and pore size dependent, as expected in layered materials. The results at the molecular scale are then used as inputs in a homogenization model to estimate the dielectric permittivity of C-S-H gel, which we compare with estimations obtained from inverse analysis based on experiments. Our results are a valuable input for multiscale modeling of non-destructive testing and evaluation in cement-based materials.

Keywords: Electromagnetic properties; Molecular Dynamics; Anisotropy; Susceptibility; Micromechanics.

1. Introduction

Dielectric permittivity measurement is one of the methods deployed for non-destructive monitoring of concrete structures [1] and to evaluate concrete property development at early ages [2, 3]. This method is sensitive to water content thanks to the dipolar character of water molecules, which feature a higher dielectric permittivity than gas and solid phases. Besides, the broadband dielectric response of porous materials also is worth measuring because it might be correlated to characteristics such as density, shrinkage, pore size distribution, and mechanical properties [4, 5, 6]. Nevertheless, assessing such characteristics requires a fundamental understanding of the dielectric response of the pore phase and microporous constituents of the material.

Several experimental studies have investigated the dielectric permittivity of cement-based materials from cement paste up to concrete scale [7, 1, 8]. Multiscale strategies have been deployed to model the complex frequency-dependent permittivity as a function of the composition [9, 10]. Micromechanics-based multiscale approaches require the knowledge of the intrinsic permittivity of the constituent phases. This property data is lacking for most of the phases in cement systems.

Calcium silicate hydrates (C-S-H) are the major hydrated phase in ordinary cement-based materials. Still, its frequency-dependent dielectric permittivity remains unknown. Guihard et al.[10] performed measurements on a mixture of C-S-H and portlandite obtained by mixing C_3S and portlandite powders with pure water. The authors estimated the dielectric permittivity of C-S-H through an inverse analysis, assuming that it is a real value that remains constant over the studied frequency range [200 MHz; 1GHz]. This assumption can be legitimately questioned since C-S-H exhibits meso- and microporosity contributing to the dielectric response over different frequency ranges. To date, to the author's knowledge, no direct experimental measurement or indirect estimate of the imaginary part of the dielectric permittivity of C-S-H exists.

The pore phase is the main contributor to the dielectric response of porous materials, with the composition of the ionic aqueous solution playing a significant role [6]. Confinement in micro- and mesopores is known to affect the dielectric response of nanoporous materials [11, 12, 13, 14]. Molecular simulations are particularly well-suited to evaluate the behavior of confined fluids under controlled composition and thermodynamic conditions. The technique has enabled quantifying how the dielectric response of confined fluids varies with the pore size [15, 13, 16]. Recently, the pore-size dependence of the static dielectric response of water confined in C-S-H has been calculated using molecular simulations [17]. It was observed that the in-plane static dielectric constant $\varepsilon_{\parallel}$ is proportional to $\exp(-h_p/13.22)$, for a pore thickness h_p in Å for C-S-H with Ca/Si of 1.7 and 1.1. The out-of-plane dielectric response of water confined in C-S-H is still to be quantified. Following the example of the density [18], hydrodynamics [19, 20] and self-diffusion [19, 20], the dielectric response is pore-size dependent [11, 12]. The computation of the frequency-dependent complex dielectric response of C-S-H is still to be addressed and can be useful to analyze the origins of the material dielectric response. Quantifying the pore size dependence of the dielectric response

*Corresponding author
Email address: sofiane.ait_hamadouche@ens-paris-saclay.fr (Sofiane Ait Hamadouche)

of C-S-H might be helpful in developing dielectric methods to measure interlayer and gel pore water content.

In this work, we perform molecular dynamics (MD) simulations to obtain the dielectric response of water confined in C-S-H at the molecular scale. To study the influence of the confinement, we consider various interlayer distances ranging from 11.8 to 106.3 Å (i.e., spanning the range of pore sizes associated with interlayer and gel pores in C-S-H). The Green-Kubo relation adapted to compute the dielectric response under a (slit) confined geometry is used. The results obtained at the molecular scale are then used as inputs in a homogenization model to estimate the frequency-dependent permittivity of C-S-H gel over a frequency range of [0 ; 1000 GHz].

2. Molecular models and methods

2.1. Dielectric response from molecular simulations

Molecular dynamics simulations enable computing the time evolution of the total dipole moment $\overrightarrow{M}(t)$, which is the sum of the dipole moment $\overrightarrow{\mu_i}(t)$ of each particle i with a charge q_i. For a system with N particles:

$$\overrightarrow{M}(t) = \sum_i^N \overrightarrow{\mu}_i(t) = \sum_i^N q_i \overrightarrow{r_i}(t) \tag{1}$$

where $\overrightarrow{r_i}(t)$ is the position of the center of the particle i.

The dielectric response of water results from microscopic relaxation processes described by the auto-correlation function of water polarization $\phi_{ij}(t)$ (for $i, j = x, y, z$) [21]:

$$\phi_{ij}(t) = \frac{\left\langle M_i(0) M_j(t) \right\rangle}{V_{cav} k_B T \varepsilon_0} \tag{2}$$

where k_B is the Boltzmann constant, T is the temperature (in Kelvin), ε_0 is the vacuum permittivity, and V_{cav} is the volume of the pore occupied by confined water. Here, this volume is computed using the sum of the Voronoï volume of the oxygen atoms in water molecules. For a Debye relaxation, $\phi_{ij}(t)$ is a simple exponential decay. Fluid-wall interaction might lead to deviations of a Debye relaxation, especially in micropores.

The frequency-dependence is computed via the Fourier transform of the components of the susceptibility tensor [22]:

$$\chi_{ij}(f) = -\int_0^\infty e^{-2\pi i f t} \frac{d\phi_{ij}(t)}{dt} dt \tag{3}$$

where f is the frequency. From Eq. (2) and (3), the susceptibility can also be written as follows [21]:

$$\chi_{ij}(f) = \phi_{ij}(0) - 2\pi i f \int_0^\infty e^{-2\pi i f t} \phi_{ij}(t) dt \tag{4}$$

The dielectric permittivity tensor $\boldsymbol{\varepsilon}$ can be computed directly from the susceptibility tensor. It must be noted that $\boldsymbol{\varepsilon}$ is neither Hermitian nor symmetrical in the general case [23]. Some simplifications can be made in the absence of an external magnetic field and considering the slit pore geometry. In a slit pore with an infinite slab of fluid confined between two walls, the dielectric tensor can be written as a function of the parallel $\varepsilon_\parallel$ and perpendicular $\varepsilon_\perp$ components [22]:

$$\boldsymbol{\varepsilon}(f) = \begin{pmatrix} \varepsilon_\parallel(f) & 0 & 0 \\ 0 & \varepsilon_\parallel(f) & 0 \\ 0 & 0 & \varepsilon_\perp(f) \end{pmatrix} \tag{5}$$

in a Cartesian frame. The frequency-dependent components of the dielectric permittivity tensor are obtained as [22]:

$$\varepsilon_\parallel(f) = 1 + \chi_\parallel(f) \tag{6}$$

$$\frac{1}{\varepsilon_\perp(f)} = 1 - \chi_\perp(f) \tag{7}$$

In the case of C-S-H, we need to check if the in-plane response - especially in small pores - can be approximated as $\varepsilon_\parallel(f) \approx \varepsilon_{xx}(f) \approx \varepsilon_{yy}(f)$. Due to translational invariance, $\varepsilon_\perp$ is expected to be negligible. Also, due to the slit geometry, the out-of-diagonal terms are expected to be $\varepsilon_{xy}(f) = \varepsilon_{yx}(f) \approx 0$. In the following, we verify the validity of these conjectures.

Finally, let us remind the usual fluctuation formula used to compute the static dielectric permittivity of isotropic fluids (e.g., [11]):

$$\varepsilon = 1 + \frac{\langle |\overrightarrow{M}|^2 \rangle - \langle |\overrightarrow{M}| \rangle^2}{3 k_B T \varepsilon_0 V} \tag{8}$$

where V is the volume of the (bulk or confined) fluid. This expression can be readily obtained from Eq. (6) and various values of $\phi_{ij}(t)$ evaluated at t =0, considering that the average dipole moment $\langle |\overrightarrow{M}| \rangle$ should be zero in an isotropic fluid.

2.2. Simulation details

The atomistic C-S-H model we use is based on Kunhi et al. [24] model with molecular formula $Ca_{1.67}SiO_{3.7}$. nH_2O. The Ca/Si of 1.67 is a common value observed in C-S-H [25, 26]. To describe the interatomic interactions, we use ClayFF [27] and SPC/E water [28]. These non-polarizable force fields have been successfully deployed to get the dielectric response of a vast range of nanoporous materials. The same atomistic modeling strategy has been used to compute the thermoelastic and interfacial properties of confined water in C-S-H [29, 30], and self-diffusion [20]. An analysis of the structural features of the C-S-H model combined with this force field is also provided in ref. [29] together with stability analysis under sorption.

To study the influence of confinement, we consider various interlayer pore sizes ranging from 11.8 to 106.3 Å (Fig. 1(A)), which spans the sizes associated with interlayer and gel pores in C-S-H as in [20]. Grand Canonical Monte Carlo (GCMC) simulations were performed to fill the system with the water content corresponding to ambient conditions and (liquid) saturated conditions (T = 300 K and RH = 100 %) (see ref. [29] for details). Two layers are simulated, therefore, two pore spaces are present in the simulated systems. One pore is kept at the equilibrium basal spacing of d_{eq} =13.7 Å, while the other is changed (see Fig. 1(A)). The following analysis deals with water present in only this second pore.

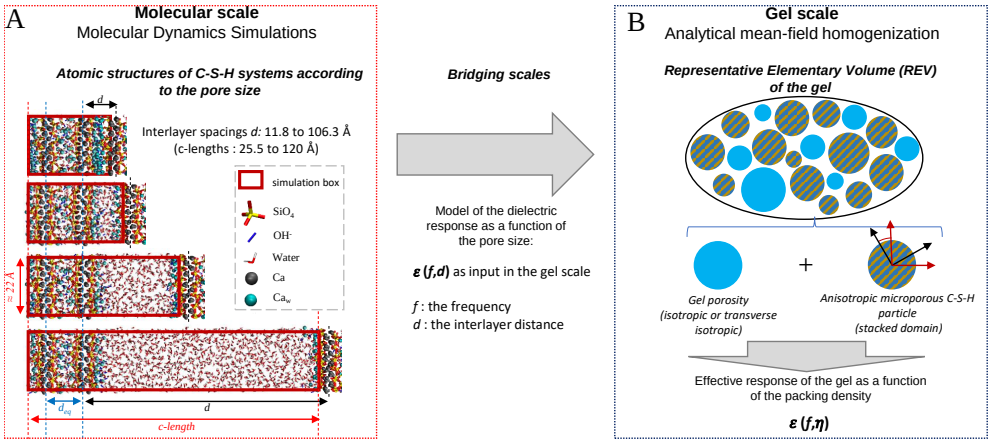

Figure 1: Multi-scale strategy adopted in this work. The dielectric response of water confined in C-S-H is computed for interlayer spacings d ranging from 11.8 to 106.3 Å. The results are then taken as inputs in a homogenization model to estimate the dielectric response at the C-S-H gel scale for diffrent packing densities η.

We use LAMMPS [31] software for MD simulations. Simulations are performed with a timestep of dt =1 fs and periodic boundary conditions. Water molecules are constrained with SHAKE algorithm [32]. For each pore size, seven configurations obtained from GCMC simulations are considered. First, a short 10 ps NVT run at T = 300 K with the Nosé-Hoover thermostat is performed, followed by a 20 ps NVE run. Production runs are then performed still in the NVE ensemble during 1 ns. The auto-correlations of dipole moments are computed with *fix ave/ correlate* in LAMMPS using input values every 10 fs, with 10000 correlation time windows accumulated, and calculating time window averages every 100 ps. Average and standard deviations are computed according to the seven different trajectories. Independent NVT simulations are performed to compute the volume cavity V_{cav} as a sum of the Voronoï volume of water oxygens in the interlayer.

Only the water and ions in the interlayer space are time integrated during MD to gain computational efficiency and reduce fluctuations in the computation of $\phi_{ij}(t)$. Since the auto-correlation function depends on the volume cavity (Eq. (2)), time-integrating the particles in the solid layer adds more considerable variability to the values of $\phi_{ij}(t)$, especially for small interlayer spacings, in which the fluctuations due to solid layer deformability are more significant compared to the total pore volume. We have compared the results of simulations with a rigid solid layer and unconstrained atoms in the solid, and the average values are similar but with more variability associated with the second case.

For the integration of $\phi_{ij}(t)$ in Eq. (3), the upper integration limit must be chosen so that the function decay is integrated correctly by avoiding the integration of noise present in the signal from the simulation [33]. Since MD simulations are based on finite differences algorithms, very long runs are prone to accumulating numerical errors, resulting in noise present in the spectra of $\phi_{ij}(t)$. To avoid the integration of that noise and to reduce the computational time needed to compute Fourier transforms in large lists, we use two equations obtained by fitting $\phi_{ij}(t)$:

- A simple exponential decay, leading to a Debye relaxation microscopically:

$$\phi_{ii}^{Deb}(t) = \varepsilon_s \exp\left[-t/\tau_{Deb}\right] \tag{9}$$

- A polynomial exponentially decaying aiming to capture potential oscillations in the $\phi(t)$ profiles:

$$\phi_{ii}^{Poly}(t) = \varepsilon_s \exp\left[-t/\tau_{Poly}\right]\left(a_0 + a_1 t + a_2 t^2 + a_3 t^3\right) \tag{10}$$

where ε_s is the static dielectric permittivity, τ_{Deb} and τ_{Poly} the relaxation time for each model, respectively. We provide results up to 1000 GHz which allows capturing the decrease in the imaginary response in the case of bulk water. It is noteworthy that physical phenomena involving smaller scales may arise at higher frequencies [34, 35]. The use of classical molecular simulation with non-polarizable force fields cannot of course capture the effects associated with electron polarization. The results above a few hundreds of gigahertz presented herein must be considered as the the contribution of the water polarization only.

3. Upscaling the dielectric permittivity

3.1. C-S-H gel microstructure representation

We adopt a microstructure representation of C-S-H gel, assuming that it is composed of two phases: microporous solid particles and gel porosity. The former is depicted as a transverse isotropic inclusion composed of C-S-H layers stacked according to the equilibrium basal spacing d_{eq} = 13.7 Å, which should be the most prevalent configuration in stacked systems [29]. The gel porosity might also be considered to exhibit a transverse isotropic or a full isotropic behavior. Various conventions are used in the literature to classify the different types of porosity in C-S-H according to their sizes. Qomi et al. [36] consider the size of the gel porosity ranging from 0.5 nm to 8 nm, while Nguyen-Tuan et al.[37] define it as ranging between 1.5 nm and 10 nm. Jennings[38] proposed two characteristic

pore sizes for C-S-H gel porosity from small-angle scattering experimental data: small gel pores [1-3 nm] and larger gel pores [3-12 nm]. In this study, to upscale C-S-H gel properties, we adopt four characteristic pore diameters spanning the typical range of gel pore sizes: 2, 3, 4 and 10 nm.

Thus, we use as input the information obtained from molecular simulations regarding the interlayer distances of 1.37 nm ($=d_{eq}$) for the solid particles and 2, 3, 4, and 10 nm for the gel pore (Fig. 1(B)). Other gel pore sizes can easily be tested. To this aim, in the following we provide expressions that fit the behavior at the molecular scale, and a homogenization scheme.

3.2. Micromechanical model

Analytical micromechanics schemes are used to upscale the dielectric permittivity of C-S-H gel, as it was recently done for mass transport properties [20, 39]. By mathematical analogy, the homogenization formula derived for upscaling the diffusivity and (thermal and electrical) conductivities can also be used to estimate the dielectric permittivity [40].

The following formula enables estimating the effective dielectric permittivity of a macroscopically isotropic heterogeneous material composed of N (microscopically) anisotropic ellipsoids is (e.g. [40]):

$$\boldsymbol{\varepsilon}^{hom} = \sum_{i=1}^{N} f_i \boldsymbol{\varepsilon}_i \mathbf{A}_i \tag{11}$$

where f_i, $\boldsymbol{\varepsilon}_i$ and $\mathbf{A}_i$ are respectively the volume fraction, dielectric permittivity tensor, and the localization tensor of phase i. The above expression can be written as a sum, provided that the dielectric behavior per phase (or pore size) is constant.

The localization tensor $\mathbf{A}$ can be approximated using the strategy proposed for the thermal conductivity [41] inspired by the Eshelby [42] solution in elasticity. In the case of elliptical inclusions randomly distributed and oriented in a representative elementary volume (REV), and under the assumption of the self-consistent (or Bruggeman) scheme (i.e., that the homogenized medium function and the reference medium mediating inclusion interactions), we get [20]:

$$\mathbf{A}_i^{SC} = \mathbf{A}_i^d \Big(\sum_{r=1}^{N} f_r \mathbf{A}_r^d\Big)^{-1} \approx \mathbf{A}_i \tag{12}$$

where $\mathbf{A}_i^d = (\mathbf{I} + \mathbf{S}_i^E((\boldsymbol{\varepsilon}^{hom})^{-1}\mathbf{R}\boldsymbol{\varepsilon}_i\mathbf{R}^T - \mathbf{I}))^{-1}$ is the localization tensor in the dilute case, with $\mathbf{R}$ being the rotation matrix, $\mathbf{I}$ being the identity matrix, and $\mathbf{S}_i^E$ the components of the diagonal (second-rank) Eshelby-like tensor [41]. Assuming that all orientations of the equiaxed ("spherical") inclusions are equally possible, the expression of the homogenized dielectric permittivity for a two-phase heterogeneous material composed of transverse isotropic phases is given by the implicit equation:

$$\varepsilon^{hom} = \frac{\frac{7(1-f_g)\varepsilon_{\parallel,s}}{\varepsilon_{\parallel,s}+2\varepsilon^{hom}} + \frac{5(1-f_g)\varepsilon_{\perp,s}}{\varepsilon_{\perp,s}+\varepsilon^{hom}} - \frac{7f_g\varepsilon_{\parallel,g}}{\varepsilon_{\parallel,g}+\varepsilon^{hom}} - \frac{5f_g\varepsilon_{\perp,g}}{\varepsilon_{\perp,g}+2\varepsilon^{hom}}}{\frac{7(1-f_g)}{\varepsilon_{\parallel,s}+2\varepsilon^{hom}} + \frac{5(1-f_g)}{\varepsilon_{\perp,s}+2\varepsilon^{hom}} - \frac{7f_g}{\varepsilon_{\parallel,g}+2\varepsilon^{hom}} - \frac{5f_g}{\varepsilon_{\perp,g}+2\varepsilon^{hom}}} \tag{13}$$

where f_g represents the gel porosity, $\varepsilon_{\parallel,p} = \varepsilon_{x,p} = \varepsilon_{y,p}$, $\varepsilon_{z,p} = \varepsilon_{\perp,p}$ the subscripts $_{,s}$ and $_{,g}$ stand, respectively, for the solid C-S-H particle and gel porosity. Eq. (13) can be written in an explicit form, but the result is too lengthy to be reported here. Among the different roots, we use only the one giving positive non-complex values for the static response. This same root is used in the calculation of the full complex spectra. This general formulation allows accounting for anisotropy on the dielectric response at the gel porosity. We will discuss the relevance of this feature in Section 4.3.

4. Results

4.1. Static dielectric response at the molecular scale

Figure 2 shows the components of the dielectric permittivity tensor in the static limit. The in-plane component $\varepsilon_{\parallel}$ ($= (\varepsilon_{xx} + \varepsilon_{yy})/2$)) of the permittivity of water confined in C-S-H is pore size dependent, with bulk-like behavior for interlayer distances exceeding roughly 6 nm (approximately 5 nm if the thickness of the solids layer is discounted out) and a strong decrease in the dielectric permittivity with the confinement of water. This result was also recently observed by Masoumi et al. [17]. This decrease can be explained by water molecules near solid surfaces being subjected to forces that hinder their polarization (an effect that would be more pronounced in hydrophilic systems like C-S-H). Our results corroborate that water confined in C-S-H follows the universal reduction in the dielectric response observed for other confined fluids [15, 13, 16]. For comparison with $\varepsilon_{\parallel}$, we computed the dielectric constant of rigid bulk SPC/E water also under ambient conditions (in a simulation with 900 molecules). We obtained $\varepsilon = 71.2 \pm 2.11$ (in agreement with other simulations of SPC/E in the literature [43, 44, 33]), which is rather close to the experimental value $\varepsilon = 78.02 \pm 0.20$ (interpolated value for T = 300 K from the experimental study of [45]). For comparison, the numerical and experimental values of bulk water are depicted in Fig. 2(A). The in-plane response $\varepsilon_{\parallel}$ obtained in our simulations can be fitted with the following expression:

$$\varepsilon_{\parallel} = \varepsilon_{inf} \exp\left(-\frac{d-B}{h_{charac}}\right) \tag{14}$$

where ε_{inf} is the dielectric constant of bulk water computed using MD simulations (= 71.2), d the interlayer distance, B = 7.1 Å is a shift in the interlayer distance, and h_{charac} = 20 Å is the characteristic distance associated with the pore size dependence of the dielectric response. When $d \gg h_{charac}$, the static dielectric response of C-S-H approaches that of bulk water. A similar expression is used to fit the results of Masoumi et al.[17], and they obtained a h_{charac} in the same order (13.22 Å) (Note that these authors used a rigid SPC water model, and this water model is known to yield a lower dielectric constant when compared to rigid SPC/E water model, which in turn underestimate the dielectric constant of a few units in relative permittivity. For the same temperature, the authors obtained a static response $\varepsilon_{\parallel} = 64$ for bulk water).

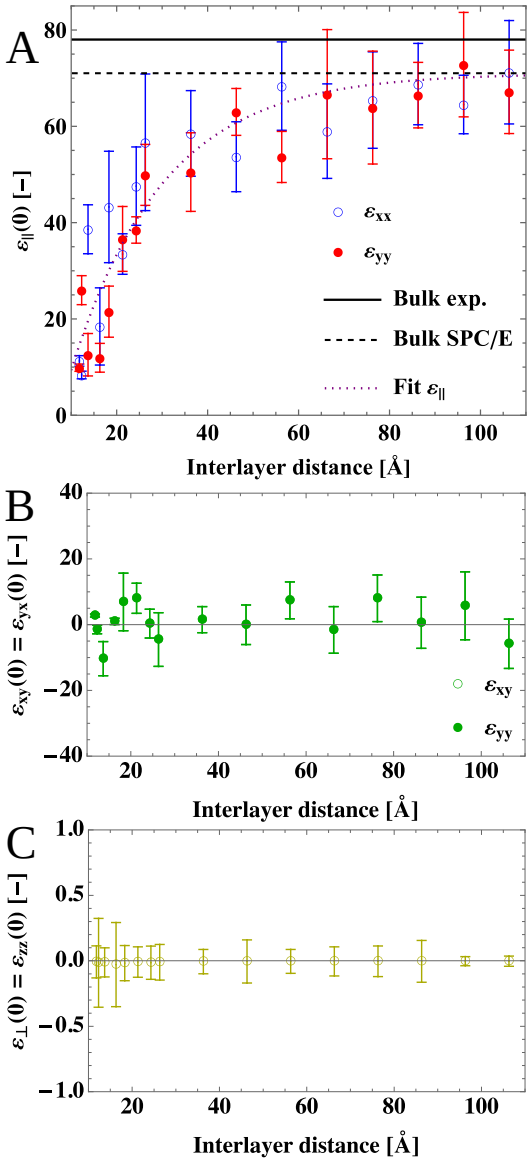

Figure 2: Components of the dielectric permittivity tensor of C-S-H at the molecular scale as a function of the interlayer distance d: (A) Parallel components ϵ_{xx}, ϵ_{yy}, and $\epsilon_{\parallel} = (\epsilon_{xx} + \epsilon_{yy})/2$ is fitted with Eq. (14) (the associated coefficients of determination regarding the values obtained from MD are R^2=0.845 for ϵ_{xx} and R^2=0.922 for ϵ_{yy}). The values for experimental and SPC/E bulk water are provided for comparison. (B) Out-of diagonal component $\epsilon_{xy} = \epsilon_{yx}$. (C) Perpendicular component $\epsilon_{\perp} = \epsilon_{zz}$.

Our results suggest some degree of anisotropy in the in-plane response, especially for interlayer distances smaller than 25 Å. Independent fits of ε_{xx} and ε_{yy} using Eq. (14) yield similar results (with coefficients of determination of R^2=0.845 and R^2=0.922, respectively). Taking into account the variability/uncertainty associated with the MD results, the approximation $\varepsilon_{\parallel} \approx \varepsilon_{xx} \approx \varepsilon_{yy}$ is reasonable.

In Figure 2(B), it can be observed that the out-of-diagonal components $\varepsilon_{xy} = \varepsilon_{yx}$ fluctuate around 0. Figure 2(C) shows that, as expected, the values of the perpendicular component $\varepsilon_{\perp}$ are negligible (with respect to the reported variability observed in the results). These results agree with the form of the dielectric tensor in Eq. (5).

4.2. *Frequency-dependent response at the molecular scale*

Figure 3 shows the polarization correlation functions of water molecules in C-S-H pores as obtained in MD simulations. The main contribution to the dielectric response comes from the parallel components ϕ_{xx}(t) and $\phi_{yy}(t)$. A significant decrease in the static value (in agreement with Fig. 2) and an increase in the relaxation time (i.e., the correlation functions go to zero at larger timescales) is observed with increasing confinement. The values of the out-of-diagonal component $\phi_{xy}(t) = \phi_{yx}(t)$ and the perpendicular component $\phi_{\perp}(t)$ indicate negligible frequency-dependent responses, as expected (see Section 2.1).

Figure 4 shows the frequency-dependent permittivity of confined water in C-S-H computed by integrating the correlation functions in Eq. (4). As discussed in Section 2.2, we fit the parallel components $\phi_{xx}(t)$ and $\phi_{yy}(t)$ using Eqs. (9) and (10) to cope with the noise in MD results and gain in precision and efficiency in the computation of integrals in Eq. (4). Both permittivity profiles obtained $\varepsilon^{Deb}(f)$ and $\varepsilon^{Poly}(f)$ are depicted in Figure 4, along with the isotropic response of bulk water provided by experimental values according to Buchner et al. [46] and simulation values using SPC/E water according to Rinne et al. [33]. In the imaginary part, we can see that the resonance frequency decreases as we increase the interlayer distance, which shows that the relaxation frequencies of bound water are lower than that of bulk water as suggested by [47].

Figure 4(C) and (F) show the difference ε_{yy} - ε_{xx} in the real and imaginary parts quantifying the possible anisotropy in the in-plane response. To quantify the anisotropy we compute the error $e_{ani} = \int_0^{\infty} |\varepsilon_{yy} - \varepsilon_{xx}| df / \int_0^{\infty} \varepsilon_{bulk} df$ using as reference the response of bulk water. With this definition, the anisotropy is **in** the order of 34 % for d = 13.7 Å, and ranges between 3 % and 22 % for the other interlayer distances, being more pronounced in the 0-10 GHz range for interlayer distances above 25 Å, and in the low frequency range for smaller pores. The anisotropy can also be evaluated in Fig. 3, where we see that for interlayer distances > 13.7, the spectra of ϕ_{yy} is inside the limits ϕ_{xx} ± standard deviation, except for d = 56.3 Å.

Regarding the choice of fitting functions for the microscopic process, while $\varepsilon^{Deb}(f)$ shows a Debye-type relaxation profile as expected, $\varepsilon^{Poly}(f)$ exhibits oscillations that may not necessarily have a physical meaning. The real part of $\varepsilon^{Poly}(f)$ have negative values around 1 GHz for d = 13.7 Å in the xx direction, whereas the dielectric permittivity of common materials (including dielectrics) is generally non-negative [48].

The results obtained so far can now be used to get an expression of the pore size dependence of the complex frequency-dependent dielectric response in C-S-H. Cole-Cole model [49], which is one of the most used relaxation models, shows a good performance in fitting $\varepsilon^{Poly}(f)$. With this model, the frequency dependence in the response reads:

$$\varepsilon^*(f) = \varepsilon_{\infty} + \frac{\varepsilon_{cc} - \varepsilon_{\infty}}{1 + (i2\pi f \tau_{cc})^{1-\alpha_{cc}}} \qquad (15)$$

where ε_{cc} and ε_{∞} are respectively the static and infinite frequency dielectric permittivity, τ_{cc} the relaxation time and α_{cc}

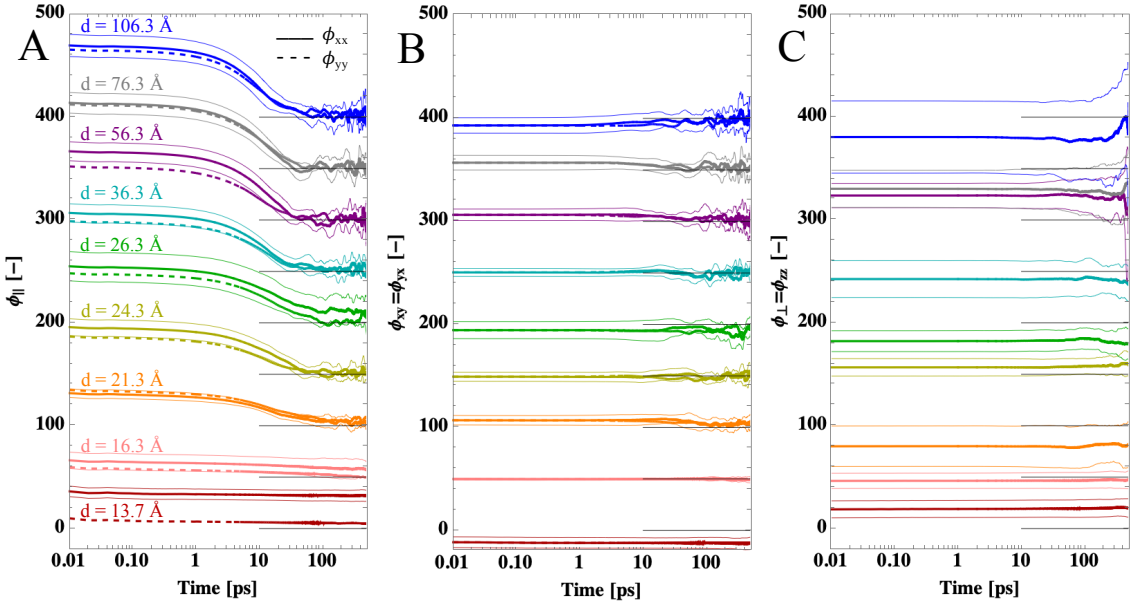

Figure 3: Polarization correlation functions of water in C-S-H for various interlayer distances: A) Parallel components ϕ_{xx} (full line), ϕ_{yy} (dashed line), (B) Out-of diagonal component $\phi_{xy} = \phi_{yx}$, and (C) Perpendicular component $\phi_{\perp} = \phi_{zz}$. The functions regarding each interlayer distance are shifted 50 units upwards for readability (the horizontal gray line marks the zero for each curve). Thin lines represent ± one standard deviation computed over the seven trajectories considered.

the exponent parameter which has a value between -1 and 1 (with $\alpha = 0$ corresponding to a Debye model). For ε_{cc}, we fixed the values of the static response obtained in Section 4.1 using Eq.(14) and ε_{∞} is taken equal to 1, since the force fields used in MD simulations do not include atomic polarization [6]. The parameters α_{cc} and τ_{cc} were determined by fitting (using least squares methods) $\varepsilon^{Poly}(f)$ with the Cole-Cole model. The Cole-Cole model does not fit the negative values, nor the bumps observed in the $\varepsilon^{Poly}(f)$ dielectric spectra. There is a good agreement between $\varepsilon^{Poly}(f)$ and the Cole-Cole fit in the real part as well as in the imaginary part (see Appendix 5).

Figure 5 depicts how Cole-Cole parameters τ_{cc} and α_{cc} vary as a function of the interlayer distance. These parameters can be fitted with the expressions below:

$$\tau_{cc} = A \exp\left(-\frac{d - A_0}{h^P_{charac}}\right) + \tau_{inf} \qquad (16)$$

$$\alpha_{cc} = -A_1\{1 - \exp\left[-A_2(d - A_3)\right]\}^2 + A_4 \qquad (17)$$

where d is the interlayer distance, $h^P_{charac} = 2.90$ Å is the characteristic distance, $\tau_{inf} = 14$ ps is the value towards which the data converge; and A, A_0, A_1, $A2$, A_3, and A_4 are other fitting coefficients whose values are reported in Table 1

The relaxation time τ_{cc} exponentially decays towards bulk water values, as expected. The relaxation frequency is the inverse of the relaxation time $\tau = 1/(2\pi f_{relaxation})$, and as discussed above, relaxation frequencies of bulk water are higher than that of bound water. Together with Eq. (14), the expressions above can be used as input in the micromechanical model aiming to estimate the dielectric response at the C-S-H gel scale.

Table 1: Coefficients of the fitting equations of α_{CC} and τ_{CC}.

Coefficients	Values
A [ps]	12655
A_0[Å]	3.33
A_1 [-]	0.589
A_2 [1/Å]	0.307
A_3 [Å]	16.046
A_4 [-]	0.673

4.3. Dielectric response of C-S-H gel

We estimate the static and frequency-dependant permittivity of C-S-H gel using Eq. (13) in accordance with the representation of the C-S-H gel structure detailed in Section 3.1. In all cases, the microporous solid particles are represented as transverse isotropic inclusions with layers stacked according to the equilibrium basal spacing $d_{eq} = 13.7$ Å. In the case of gel porosity, two cases are considered:

- A 2D response (as in Eq. 5) with $\varepsilon_{x,g}(f) = \varepsilon_{y,g}(f) = \varepsilon_{\parallel,g}(f)$, and $\varepsilon_{z,g}(f) = 0$
- An isotropic response with $\varepsilon_{x,g}(f) = \varepsilon_{y,g}(f) = \varepsilon_{z,g}(f)$

Figure 6 shows the static response of C-S-H gel $\varepsilon_{gel}(0)$ as a function of the packing density $\eta = 1 - f_g$. The filled and hollow circles at $\eta = 0.64$ and $\eta = 0.74$ refer to the static permittivity of low density (LD) and high density (HD) C-S-H, respectively, the two main packing densities of C-S-H [50]. The values of the static response of LD and HD C-S-H for the 2D and isotropic cases are summarized in Table 2. Our values are in agreement with Guihard et al. [10] reporting a static dielectric permittivity of C-S-H in the range 2-20. In this reference, these values are

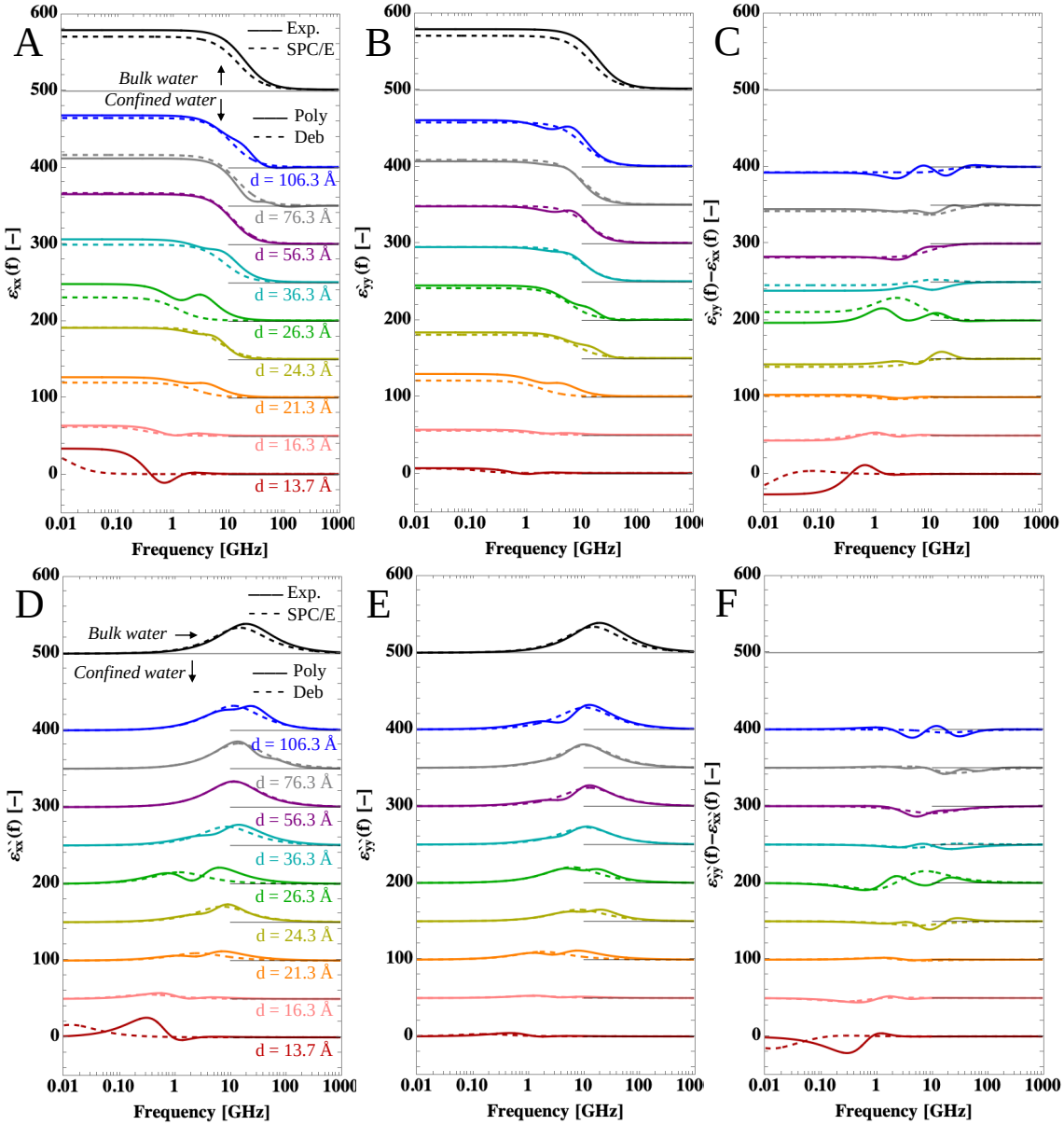

Figure 4: Dielectric permittivity of confined water in C-S-H: (A),(B) real and (D),(E) imaginary parts. The (isotropic) response of bulk water is shown for comparison (experimental values according to Buchner et al. [46] and simulation values for SPC/E water according to Rinne et al. [33]). The functions regarding each interlayer distance are shifted 50 units upwards for readability (the horizontal gray line marks the zero for each curve); bulk water values are shifted 500 units upwards. To quantify the (an)isotropy in the parallel components of the dielectric tensor, the difference $\epsilon_{yy} - \epsilon_{xx}$ is calculated for the (C) real and (D) imaginary parts of the dielectric response for selected slit pore sizes.

Table 2: Static permittivity of LD and HD C-S-H when a 2D or an isotropic behaviour is assumed for the gel porosity configurations.

	case	d_g = 2 nm	d_g = 3 nm	d_g = 4 nm	d_g = 10 nm
$\varepsilon_{gel}(0)$ (LD)	2D	8.75	9.86	10.40	11.08
$\varepsilon_{gel}(0)$ (HD)	2D	8.30	9.03	9.36	9.77
$\varepsilon_{gel}(0)$ (LD)	Iso	15.14	18.20	19.87	22.14
$\varepsilon_{gel}(0)$ (HD)	Iso	12.72	15.58	15.53	16.77

obtained through inverse analysis of experimental data in the frequency range [200 MHz; 1GHz]. Our results however show that some frequency dependency in C-S-H would arise, even at this relatively low frequency range, due to the contribution of interlayer pores as discussed below.

Figure 7 shows the frequency dependence of the effective dielectric response of C-S-H gel. It depicts the real and imaginary parts of $\varepsilon_{gel}(f)$ for both 2D and isotropic cases for gel

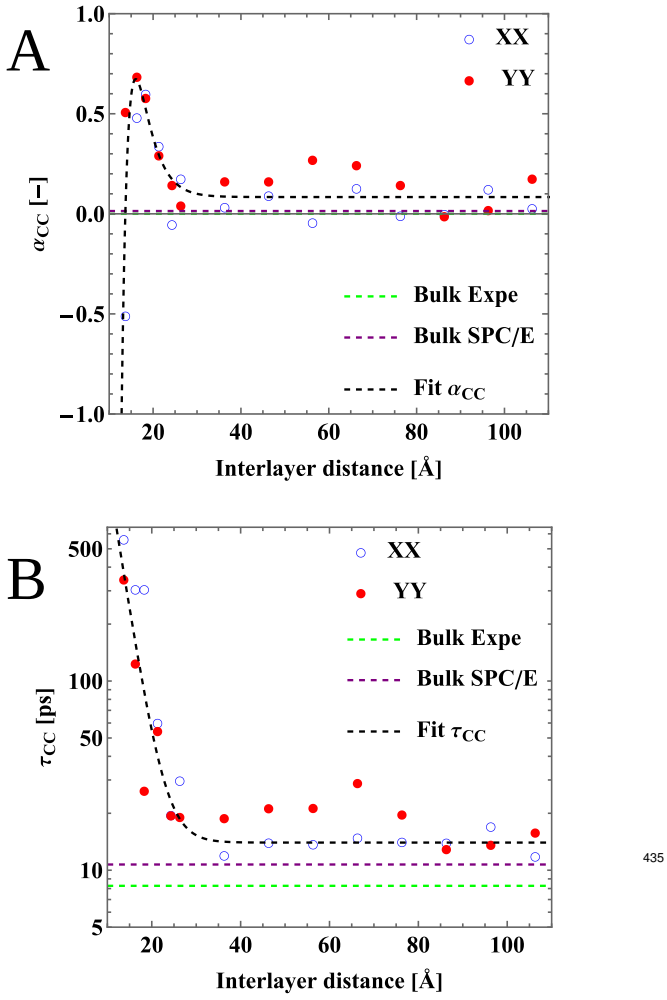

Figure 5: Variation of Cole-Cole parameters of water confined in C-S-H at the molecular scale (A) α_{cc} and (B) τ_{cc} as a function of the interlayer distance. Fits using Eqs. 16 and 17 are provided. The purple and green dashed lines represent, respectively, the Cole-Cole parameters from experiments [46] and MD simulations using the SPC/E water model [33].

porosity according to various packing densities (ranging from 0.1 to 1) and for the four characteristic gel pore sizes considered here (2, 3, 4, and 10 nm). We observe that the dielectric response at the gel scale depends the gel pore size. The dielectric response of C-S-H gel is fitted using a Cole-Cole model. As at the molecular scale, we fix the values of the static response (Fig. 6) for ε_{cc}. The variation of the two remaining Cole-Cole parameters (α_{cc} and τ_{cc}) as a function of the packing density is illustrated in Fig. 8. The behaviour of system with pores > 2 nm features the same tendency. Hence, α_{cc} and τ_{cc} presented for d_g=4 nm are also valid for mid to large pore gels. Nevertheless, the static response at d_g = 10 nm has higher values than at d_g = 4 nm, which induces differences at the frequency-dependent dielectric response (Fig. 7). Table 3 outlines α_{cc} and τ_{cc} of LD and HD C-S-H.

According to [51], confined water shows an anisotropic response ($\varepsilon_{\parallel} \neq \varepsilon_{\perp}$) in pore as large as 100 nm. The authors studied the dielectric response of water molecules confined between hydrophobic surfaces, under the influence of external electric fields. Since the nature of the surfaces between which water molecules are confined is deemed to have little influence on the dielectric response [13], we can assume that $\varepsilon_{\parallel} \neq \varepsilon_{\perp}$ in the gel porosity of our hydrophilic system, and therefore we consider the 2D case as the more relevant.

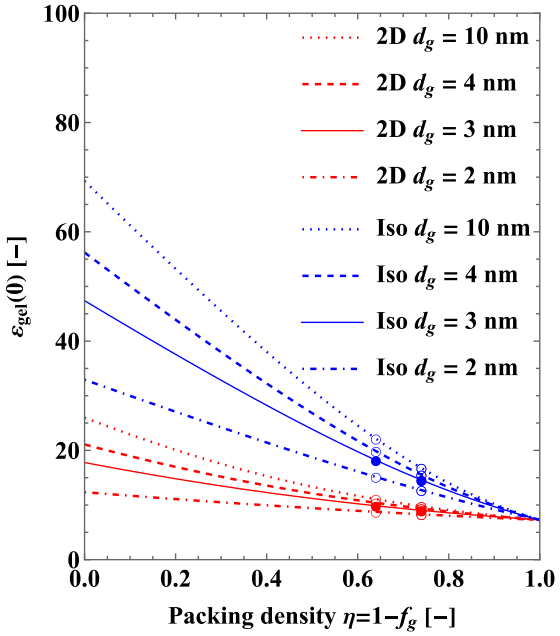

Figure 6: Static response of C-S-H gel as a function of the packing density.

5. Conclusion

In this work, we computed the dielectric response of water confined in C-S-H at the molecular scale using MD simulations. These results were used as input in a micromechanical model in order to get the response at the gel scale. Our results provide valuable input for the multiscale modeling of dielectric permittivity of cement-based materials, estimating the intrinsic frequency-dependent permittivity of C-S-H gel for the first time. The main conclusions are:

- *Dielectric response of confined water in C-S-H at the molecular scale*. The static dielectric response of water confined in C-S-H decreases with confinement, confirming that the universal reduction in the dielectric response of confined fluids [15, 13, 16, 17] is also valid for C-S-H. For interlayer distances above roughly 6 nm, the dielectric response retrieves that of bulk water. The parallel component of frequency-dependent dielectric permittivity of confined water in C-S-H is adequately fitted by a Cole-Cole model with parameters depending on the pore size.

- *Anisotropy in the dielectric response at the molecular scale*. Both pore in-plane directions (x and y) show a

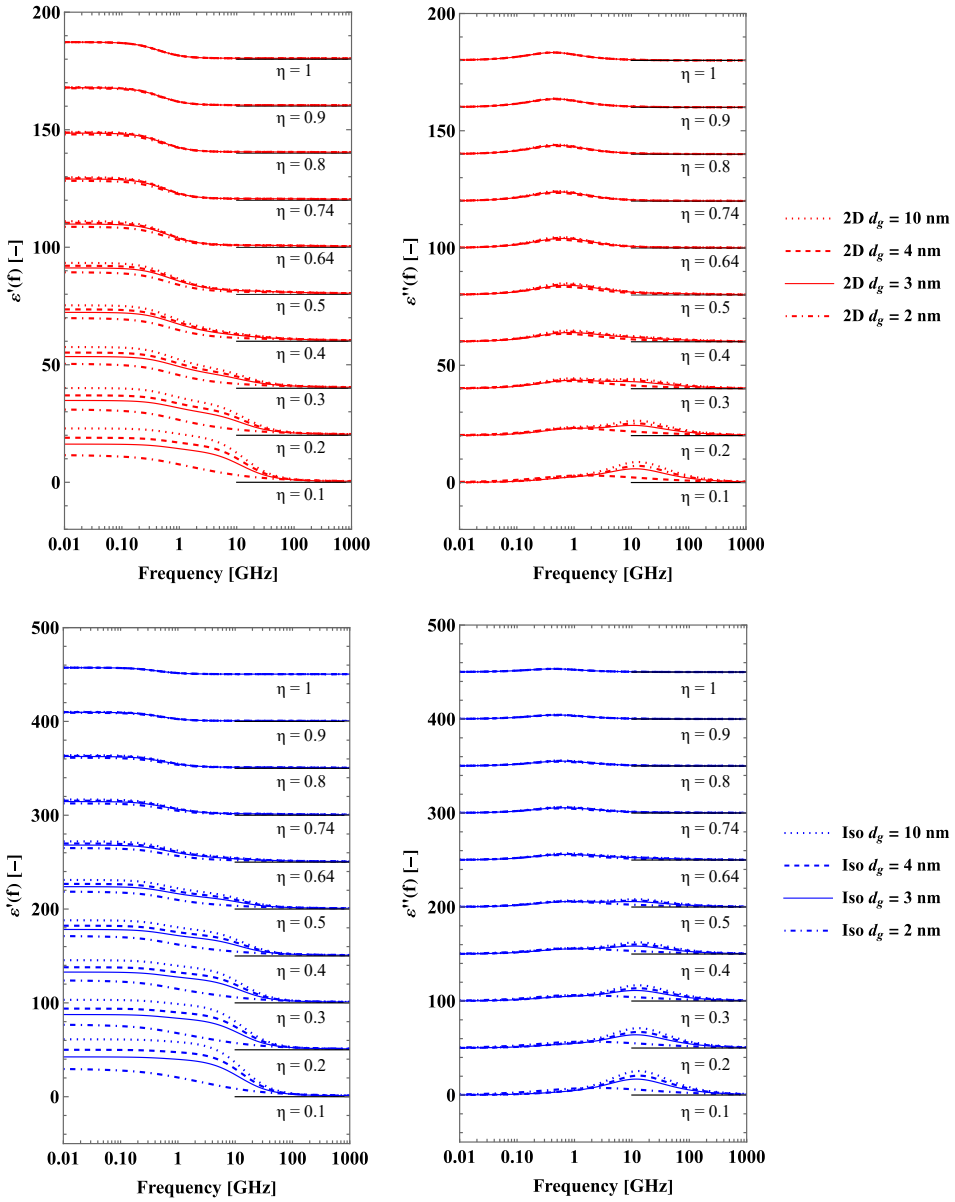

Figure 7: Frequency dependent dielectric response of C-S-H gel considering 2 cases for the response of the gel porosity ε_g: (A) a 2D response i.e. $\varepsilon_{x,g} = \varepsilon_{y,g} = \varepsilon_{\parallel,g}$ while $\varepsilon_{z,g} = \varepsilon_{\perp,g} = 0$ and (B) considering an isotropic response i.e. $\varepsilon_{\parallel,g} = \varepsilon_{\perp,g}$. The graphics for each packing density are shifted upwards 15 units in (A) and 40 units in (B) for readability..

Table 3: Cole-Cole parameters of LD and HD C-S-H.

	case	d_g = 2 nm	d_g = 3 nm	d_g = 4 nm	d_g = 10 nm
α_{cc} [-] (LD)	2D	0.024	0.041	0.048	0.051
τ_{cc} [ps] (LD)	2D	281	243	245	251
α_{cc} [-] (HD)	2D	0.018	0.017	0.016	0.016
τ_{cc} [ps] (HD)	2D	312	289	293	299
α_{cc} [-] (LD)	Iso	0.212	0.279	0.297	0.306
τ_{cc} [ps] (LD)	Iso	211	127	121	116
α_{cc} [-] (HD)	Iso	0.118	0.145	0.152	0.153
τ_{cc} [ps] (HD)	Iso	259	207	206	208

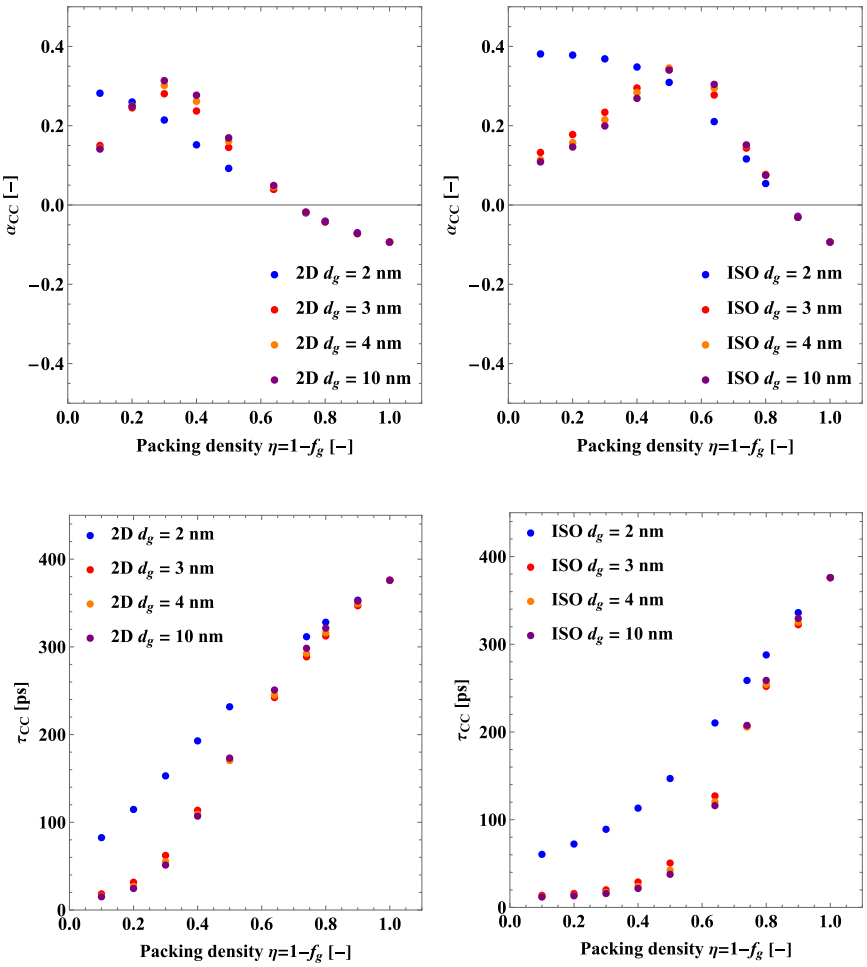

Figure 8: Variation of Cole-Cole parameters obtained from fitting the effective dielectric response of C-S-H gel as a function of the packing density η.

similar response, which justifies attributing a transverse isotropic behavior to C-S-H at the molecular scale, and that even for small interlayer pores. The perpendicular component of the dielectric tensor vanishes, which indicates a reduction in the dimensionality at the molecular level. Evidence from the study of water confined in large mesopores suggests that the anisotropic character of the response persists up to pore sizes as large as 100 nm [51], which justifies adopting a transverse isotropic behavior even for gel pores. The out-of-diagonal components of the dielectric tensor are shown to fluctuate around 0. Accounting for the anisotropy at the molecular level is critical in determining the response of C-S-H.

- *Dielectric response of C-S-H gel.* We quantify the complex dielectric response of C-S-H as a function of the packing density, which is input for multiscale approaches coping with C-S-H densification [52]. The values of the static response of LD and HD C-S-H are in the range of 2-20 identified in experimental studies [10]. The Cole-Cole model also fits pretty well the results at the gel scale. In our analysis, we considered various gel pore sizes. Our results provide, therefore, a full characterization of the variability of the complex dielectric response of C-S-H gel, accounting for the entire range of packing density and gel pore sizes. In future micromechanical modeling of the dielectric properties of cement-based materials, C-S-H must be considered as a phase showing a complex frequency-dependent behavior.

The perspective of this work includes considering the effect of unsaturated pores and also applying the multiscale strategy to other hydrates/ microporous phases in cement systems (e.g., AF-phases).

Acknowledgement

This work has benefited from the financial support of the LabEx LaSIPS (ANR-10-LABX-0032-LaSIPS) managed by the French National Research Agency under the "Investissements d'avenir" program (ANR-11-IDEX-0003).

Appendix. Correlation between ε^{Poly} and the Cole-Cole fit

Figure 9 shows fittings of autocorrelation functions ϕ_{xx} and ϕ_{yy} using simple exponential decay and polynomial exponentially decaying for selected interlayer distances. The associated quality of fittings is assessed according to the determination coefficient (R^2) and overall standard deviation (in relative dielectric permittivity units). Overall, polynomial fits yield a better R^2 and lower standard deviation than the exponential decay.

Figure 10 shows the coefficient of determination R^2 between the Cole-Cole fit of the dielectric response at the molecular scale for both real and imaginary parts. The R^2 values are all above 0.9 for interlayer distances above 3 nm. For smaller pores, the R^2 are lower but remain in the domain of good correlation.

References

[1] C. Andrade, V. M. Blanco, A. Collazo, M. Keddam, X. R. Nóvoa, H. Takenouti, Cement paste hardening process studied by impedance spectroscopy, Electrochimica Acta 44 (24) (1999) 4313–4318.

[2] Van Beek, A., Milhorst, M.A., Dielectric measurements to characterize the microstructural changes of young concrete, HERON, vol. 44 (1), 2000 (Jan. 2000).

[3] X. Z. Ding, X. Zhang, C. K. Ong, B. T. G. Tan, J. Yang, Study of dielectric and electrical properties of mortar in the early hydration period at microwave frequencies, Journal of Materials Science 31 (20) (1996) 5339–5345.

[4] S. Tang, X. Cai, Z. He, W. Zhou, H. Shao, Z. Li, T. Wu, E. Chen, The review of early hydration of cement-based materials by electrical methods, Construction and Building Materials 146 (2017) 15–29. doi:10.1016/j.conbuildmat.2017.04.073.
URL https://linkinghub.elsevier.com/retrieve/pii/S0950061817307262

[5] V. P. Drnevich, A. K. Ashmawy, X. Yu, A. M. Sallam, Time domain reflectometry for water content and density of soils: study of soil-dependent calibration constants, Canadian Geotechnical Journal 42 (4) (2005) 1053–1065. doi:10.1139/t05-047.
URL https://www.nrcresearchpress.com/doi/abs/10.1139/t05-047

[6] T. Honorio, T. Bore, F. Benboudjema, E. Vourc'h, M. Ferhat, Dielectric properties of the pore solution in cement-based materials, Journal of Molecular Liquids 302 (2020) 112548.

[7] V. Guihard, F. Taillade, J.-P. Balayssac, B. Steck, J. Sanahuja, F. Deby, Permittivity measurement of cementitious materials with an open-ended coaxial probe, Construction and Building Materials 230 (2020) 116946. doi:10.1016/j.conbuildmat.2019.116946.
URL https://www.sciencedirect.com/science/article/pii/S0950061819323888

[8] P. R. Camp, S. Bilotta, Dielectric properties of portland cement paste as a function of time since mixing, Journal of Applied Physics 66 (12) (1989) 6007–6013, publisher: American Institute of Physics. doi:10.1063/1.343577.
URL https://aip.scitation.org/doi/citedby/10.1063/1.343577

[9] V. Guihard, F. Taillade, J. P. Balayssac, B. Steck, J. Sanahuja, F. Deby, Prediction of Cement-Based Materials' Water Content with the Use of Electromagnetic Homogenisation Schemes, in: 2018 Progress in Electromagnetics Research Symposium (PIERS-Toyama), 2018, pp. 164–168, iSSN: 1559-9450. doi:10.23919/PIERS.2018.8597698.

[10] V. Guihard, C. Patapy, J. Sanahuja, J.-P. Balayssac, F. Taillade, B. Steck, Effective medium theories in electromagnetism for the prediction of water content in cement pastes, International Journal of Engineering Science 150 (2020) 103273. doi:10.1016/j.ijengsci.2020.103273.
URL https://www.sciencedirect.com/science/article/pii/S0020722520300616

[11] V. Ballenegger, J.-P. Hansen, Dielectric permittivity profiles of confined polar fluids, The Journal of Chemical Physics 122 (11) (2005) 114711.

[12] D. J. Bonthuis, S. Gekle, R. R. Netz, Dielectric Profile of Interfacial Water and its Effect on Double-Layer Capacitance, Physical Review Letters 107 (16) (Oct. 2011).

[13] C. Zhang, F. Gygi, G. Galli, Strongly Anisotropic Dielectric Relaxation of Water at the Nanoscale, The Journal of Physical Chemistry Letters 4 (15) (2013) 2477–2481.

[14] L. Fumagalli, A. Esfandiar, R. Fabregas, S. Hu, P. Ares, A. Janardanan, Q. Yang, B. Radha, T. Taniguchi, K. Watanabe, G. Gomila, K. S. Novoselov, A. K. Geim, Anomalously low dielectric constant of confined water, Science 360 (6395) (2018) 1339–1342.

[15] S. Senapati, A. Chandra, Dielectric Constant of Water Confined in a Nanocavity, The Journal of Physical Chemistry B 105 (22) (2001) 5106–5109, publisher: American Chemical Society. doi:10.1021/jp011058i.
URL https://doi.org/10.1021/jp011058i

[16] M. H. Motevaselian, N. R. Aluru, Universal Reduction in Dielectric Response of Confined Fluids, ACS Nano 14 (10) (2020) 12761–12770. doi:10.1021/acsnano.0c03173.
URL https://pubs.acs.org/doi/10.1021/acsnano.0c03173

[17] S. Masoumi, S. Zare, H. Valipour, M. J. Abdolhosseini Qomi, Effective Interactions between Calcium-Silicate-Hydrate Nanolayers, The Journal of Physical Chemistry C 123 (8) (2019) 4755–4766.

[18] T. Honorio, Monte Carlo Molecular Modeling of Temperature and Pressure Effects on the Interactions between Crystalline Calcium Silicate Hydrate Layers, Langmuir 35 (11) (2019) 3907–3916.

[19] A. Botan, B. Rotenberg, V. Marry, P. Turq, B. Noetinger, Hydrodynamics in Clay Nanopores, The Journal of Physical Chemistry C 115 (32) (2011) 16109–16115.

[20] T. Honorio, H. Carasek, O. Cascudo, Water self-diffusion in C-S-H: Effect of confinement and temperature studied by molecular dynamics, Cement and Concrete Research 155 (2022) 106775. doi:10.1016/j.cemconres.2022.106775.
URL https://www.sciencedirect.com/science/article/pii/S0008884622000667

[21] R. Kf, G. S, N. Rr, Ion-specific solvation water dynamics: single water versus collective water effects, The journal of physical chemistry. A 118 (50), publisher: J Phys Chem A (Dec. 2014). doi:10.1021/jp5066874.
URL https://pubmed.ncbi.nlm.nih.gov/25474321/

[22] V. A. Froltsov, S. H. L. Klapp, Dielectric response of polar liquids in narrow slit pores, The Journal of Chemical Physics 126 (11) (2007) 114703. doi:10.1063/1.2566913.
URL https://aip.scitation.org/doi/full/10.1063/1.2566913

[23] V. M. Agranovich, V. Ginzburg, Crystal Optics with Spatial Dispersion, and Excitons, Vol. 42 of Springer Series in Solid-State Sciences, Springer Berlin Heidelberg, Berlin, Heidelberg, 1984. doi:10.1007/978-3-662-02406-5.
URL http://link.springer.com/10.1007/978-3-662-02406-5

[24] A. Kunhi Mohamed, S. C. Parker, P. Bowen, S. Galmarini, An atomistic building block description of C-S-H - Towards a realistic C-S-H model, Cement and Concrete Research 107 (2018) 221–235.

[25] I. G. Richardson, Tobermorite/jennite- and tobermorite/calcium hydroxide-based models for the structure of C-S-H: applicability to hardened pastes of tricalcium silicate, β-dicalcium silicate, Portland cement, and blends of Portland cement with blast-furnace slag, metakaolin, or silica fume, Cement and Concrete Research 34 (9) (2004) 1733–1777.

[26] A. J. Allen, J. J. Thomas, H. M. Jennings, Composition and density of nanoscale calcium–silicate–hydrate in cement, Nature Materials 6 (4) (2007) 311–316.

[27] R. T. Cygan, J.-J. Liang, A. G. Kalinichev, Molecular Models of Hydroxide, Oxyhydroxide, and Clay Phases and the Development of a General Force Field, The Journal of Physical Chemistry B 108 (4) (2004) 1255–1266.

[28] H. J. C. Berendsen, J. R. Grigera, T. P. Straatsma, The missing term in effective pair potentials, The Journal of Physical Chemistry 91 (24) (1987) 6269–6271.

[29] T. Honorio, F. Masara, F. Benboudjema, Heat capacity, isothermal compressibility, isosteric heat of adsorption and thermal expansion of water

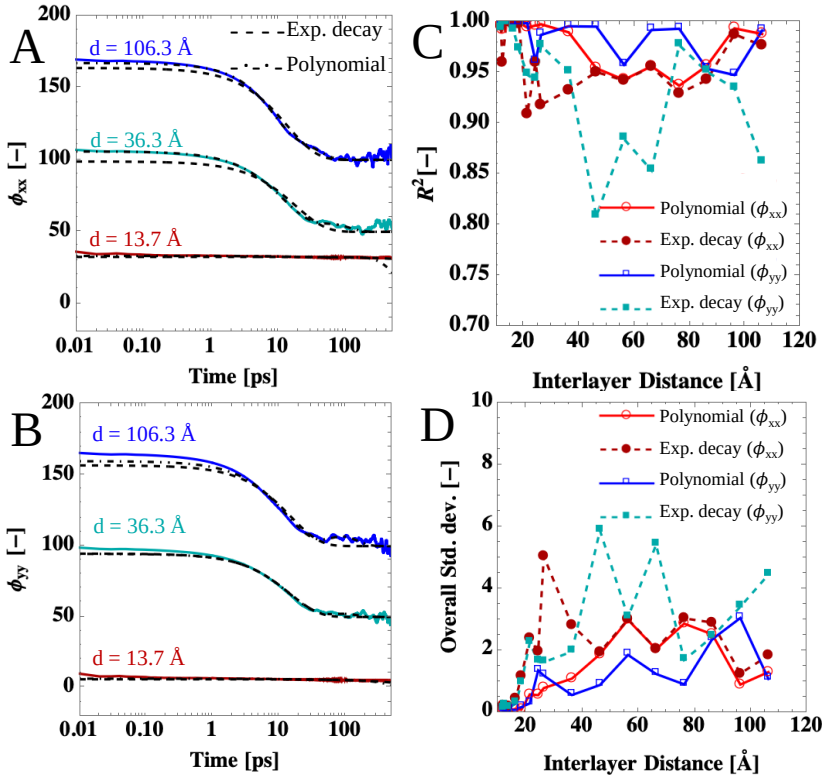

Figure 9: Fitting of autocorrelation functions (A) ϕ_{xx} and (B) ϕ_{yy} using simple exponential decay (dashed lines) and polynomial exponentially decaying (dot-dashed lines) for selected interlayer distances. The associated quality of fittings is assessed according to (C) determination coefficient (R^2) and (D) overall standard deviation (in relative dielectric permittivity units).

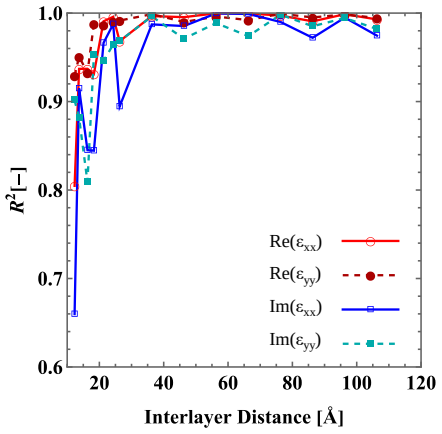

Figure 10: The coefficient of determination R^2 between the Cole-Cole fit and the real and imaginary parts of $\varepsilon_{xx}^{Poly}(f)$ and $\varepsilon_{yy}^{Poly}(f)$ as a function of the interlayer distances.

confined in C-S-H, Cement 6 (2021) 100015. doi:10.1016/j.cement.2021.100015.
URL https://www.sciencedirect.com/science/article/pii/S2666549221000128

[30] F. Masara, T. Honorio, F. Benboudjema, Sorption in C-S-H at the molecular level: Disjoining pressures, effective interactions, hysteresis, and cavitation, Cement and Concrete Research 164 (2023) 107047. doi:10.1016/j.cemconres.2022.107047.
URL https://www.sciencedirect.com/science/article/pii/S0008884622003398

[31] S. Plimpton, Fast Parallel Algorithms for Short-Range Molecular Dynamics, Journal of Computational Physics 117 (1) (1995) 1–19. doi:10.1006/jcph.1995.1039.
URL http://www.sciencedirect.com/science/article/pii/S002199918571039X

[32] J.-P. Ryckaert, G. Ciccotti, H. J. Berendsen, Numerical integration of the cartesian equations of motion of a system with constraints: molecular dynamics of n-alkanes, Journal of Computational Physics 23 (3) (1977) 327–341. doi:10.1016/0021-9991(77)90098-5.
URL https://linkinghub.elsevier.com/retrieve/pii/0021999177900985

[33] K. F. Rinne, S. Gekle, R. R. Netz, Dissecting ion-specific dielectric spectra of sodium-halide solutions into solvation water and ionic contributions, The Journal of Chemical Physics 141 (21) (2014) 214502. doi:10.1063/1.4901927.
URL http://aip.scitation.org/doi/10.1063/1.4901927

[34] H. Yada, M. Nagai, K. Tanaka, Origin of the fast relaxation component of water and heavy water revealed by terahertz time-domain attenuated total reflection spectroscopy, Chemical Physics Letters 464 (4) (2008) 166–170. doi:10.1016/j.cplett.2008.09.015.
URL https://www.sciencedirect.com/science/article/pii/S0009261408012487

[35] G. Brodie, Modeling the very broad band dielectric properties of water, Journal of Microwave Power and Electromagnetic Energy 55 (1) (2021) 80–89, publisher: Taylor & Francis _eprint: https://doi.org/10.1080/08327823.2021.1877243. doi:10.1080/08327823.2021.1877243.
URL https://doi.org/10.1080/08327823.2021.1877243

[36] M. J. Abdolhosseini Qomi, L. Brochard, T. Honorio, I. Maruyama, M. Vandamme, Advances in atomistic modeling and understanding of drying shrinkage in cementitious materials, Cement and Concrete Research 148 (2021) 106536. doi:10.1016/j.cemconres.2021.106536.

URL https://www.sciencedirect.com/science/article/pii/S000888462100185X

[37] L. Nguyen-Tuan, M. A. Etzold, C. Rößler, H.-M. Ludwig, Growth and porosity of C-S-H phases using the sheet growth model, Cement and Concrete Research 129 (2020) 105960. doi:10.1016/j.cemconres.2019.105960.
URL https://www.sciencedirect.com/science/article/pii/S0008884619306428

[38] H. M. Jennings, Refinements to colloid model of C-S-H in cement: CM-II, Cement and Concrete Research 38 (3) (2008) 275–289. doi:10.1016/j.cemconres.2007.10.006.
URL https://www.sciencedirect.com/science/article/pii/S0008884607002761

[39] T. Honorio, Permeability of C-S-H (Jun. 2022). doi:10.2139/ssrn.4132286.
URL https://papers.ssrn.com/abstract=4132286

[40] S. Torquato, Random Heterogeneous Materials: Microstructure and Macroscopic Properties, Springer Science & Business Media, 2002.

[41] H. Hatta, M. Taya, Effective thermal conductivity of a misoriented short fiber composite, Journal of Applied Physics 58 (7) (1985) 2478–2486. doi:10.1063/1.335924.
URL http://aip.scitation.org/doi/10.1063/1.335924

[42] J. Eshelby, Progress in solid mechanics: Vol. 1. Edited by IN Sneddon and R. Hill, North-Holland Publishing Company, Amsterdam, 1960, 448 pp., 100s (1961).

[43] M. Rami Reddy, M. Berkowitz, The dielectric constant of SPC/E water, Chemical Physics Letters 155 (2) (1989) 173–176. doi:10.1016/0009-2614(89)85344-8.
URL https://www.sciencedirect.com/science/article/pii/0009261489853448

[44] R. Fuentes-Azcatl, N. Mendoza, J. Alejandre, Improved SPC force field of water based on the dielectric constant: SPC/ϵ, Physica A: Statistical Mechanics and its Applications 420 (2015) 116–123. doi:10.1016/j.physa.2014.10.072.
URL https://www.sciencedirect.com/science/article/pii/S0378437114009108

[45] A. P. Gregory, R. N. Clarke, Traceable measurements of the static permittivity of dielectric reference liquids over the temperature range 5–50 °C, Measurement Science and Technology 16 (7) (2005) 1506. doi:10.1088/0957-0233/16/7/013.
URL https://dx.doi.org/10.1088/0957-0233/16/7/013

[46] R. Buchner, G. T. Hefter, P. M. May, Dielectric Relaxation of Aqueous NaCl Solutions, The Journal of Physical Chemistry A 103 (1) (1999) 1–9. doi:10.1021/jp982977k.
URL http://pubs.acs.org/doi/abs/10.1021/jp982977k

[47] M. C. Dobson, F. T. Ulaby, M. T. Hallikainen, M. A. El-rayes, Microwave Dielectric Behavior of Wet Soil-Part II: Dielectric Mixing Models, IEEE Transactions on Geoscience and Remote Sensing GE-23 (1) (1985) 35–46, conference Name: IEEE Transactions on Geoscience and Remote Sensing. doi:10.1109/TGRS.1985.289498.

[48] G. Fan, K. Sun, Q. Hou, Z. Wang, Y. Liu, R. Fan, Epsilon-negative media from the viewpoint of materials science, EPJ Applied Metamaterials 8 (2021) 11, publisher: EDP Sciences. doi:10.1051/epjam/2021005.
URL https://epjam.edp-open.org/articles/epjam/abs/2021/01/epjam200025/epjam200025.html

[49] K. S. Cole, R. H. Cole, Dispersion and Absorption in Dielectrics I. Alternating Current Characteristics, The Journal of Chemical Physics 9 (4) (1941) 341–351, publisher: American Institute of Physics. doi:10.1063/1.1750906.
URL https://aip.scitation.org/doi/10.1063/1.1750906

[50] G. Constantinides, F.-J. Ulm, The effect of two types of C-S-H on the elasticity of cement-based materials: Results from nanoindentation and micromechanical modeling, Cement and Concrete Research 34 (1) (2004) 67–80. doi:10.1016/S0008-8846(03)00230-8.
URL https://www.sciencedirect.com/science/article/pii/S0008884603002308

[51] S. De Luca, S. K. Kannam, B. D. Todd, F. Frascoli, J. S. Hansen, P. J. Daivis, Effects of Confinement on the Dielectric Response of Water Extends up to Mesoscale Dimensions, Langmuir 32 (19) (2016) 4765–4773, publisher: American Chemical Society. doi:10.1021/acs.langmuir.6b00791.
URL https://doi.org/10.1021/acs.langmuir.6b00791

[52] A. C. A. Muller, K. L. Scrivener, A. M. Gajewicz, P. J. McDonald, Densification of C–S–H Measured by 1H NMR Relaxometry, The Journal of Physical Chemistry C 117 (1) (2012) 403–412.